 CMC, vol.37, no.2, pp.109-121, 2013

Broadbanding of A-sandwich Radome Using Jerusalem Cross Frequency Selective Surface

Raveendranath U Nair[1] **and R M Jha**[1]

Abstract: Enhancement of electromagnetic performance of A-sandwich radome using aperture-type Jerusalem cross frequency selective surface (FSS) is presented. The Jerusalem cross FSS array is embedded in the mid-plane of the core of A-sandwich radome to enhance the EM performance parameters over the entire X-band. For modeling the Jerusalem cross FSS embedded radome panel and evaluation of its EM performance parameters, equivalent transmission line method in conjunction with equivalent circuit model is used. A comparative study of Jerusalem cross FSS embedded A-sandwich radome and A-sandwich radome of identical material and thickness (core and skin layers) indicate that the new wall configuration has superior EM performance as compared to the A-sandwich wall alone configuration. The excellent EM performance of Jerusalem cross FSS embedded A-sandwich radome makes it a desirable choice for the design of normal incidence radomes (hemispherical/ cylindrical), near-normal incidence radomes (paraboloidal) and highly streamlined airborne nosecone radomes.

Keywords: Frequency selective surfaces, A-sandwich radome, Equivalent transmission line model.

1 Introduction

In order to enhance the radome electromagnetic (EM) performance parameters, several techniques have been reported [Cary (1983); Kozakoff (2010)]. Metallic wire grids/ wire meshes were used for broadbanding of thin dielectric slabs. In some of the earlier works, perforated metallic resonant wall structures were embedded within the radome panel or fixed behind the radome panel for broadbanding applications. Periodic array of conducting inclusions was centrally loaded in a monolithic radome for obtaining wider bandwidth [Frenkel (2001)]. High transmission efficiency, very low cross-polar levels, and minimal boresight error are the desired major radome EM performance parameters over wideband of frequencies.

[1] CSIR-National Aerospace Laboratories, Bangalore, 560017, India.

In the previously reported works, superior power transmission characteristics have been achieved at the cost of other performance parameters like boresight error, cross-polar level, which may degrade drastically. It demands the development of novel radome design techniques, which can simultaneously improve the EM performance parameters of radome walls. For such applications, frequency selective surface (FSS) based radome wall structures are desirable [Wu (1995); Munk (2005); Lin *et al*. (2009); Costa and Monorchio (2012)]. Recently, metamaterial based FSS are widely used in the design of novel radome configurations [Cory *et al*. (2007); Latrach *et al*. (2010); Basiry *et al*. (2011); Choudhury *et al*. (2012); Narayan *et al*. (2012)].

A-sandwich radome wall configuration is generally preferred in airborne radome applications due to its high strength-to-weight ratio and large bandwidth. But the major drawback of A-sandwich wall is the degradation of EM performance parameters at high incidence angles. In the present work, application of Jerusalem cross FSS for enhancement radome performance parameters over X-band for a given set of incidence angles (0°, 45°, and 80°) is presented in view of possible applications in the design of hemispherical, paraboloidal and highly streamlined nosecone radomes. The present work is an extension of our earlier reported work [Nair and Jha (2012)]. Further, detailed EM design and performance analysis of Jerusalem cross FSS embedded A-sandwich radome is carried out based on equivalent transmission line method in conjunction with equivalent circuit model.

For the A-sandwich radome panel considered, the core thickness is optimized for power transmission over the entire X-band. Then aperture-type Jerusalem cross FSS array is embedded in the mid-plane of the core to enhance the EM performance parameters of the A-sandwich radome panel over X-band. EM performance analysis shows that Jerusalem cross FSS embedded A-sandwich panel has superior EM performance as compared to the A-sandwich radome panel alone.

2 EM Design Aspects

A pair of crossed dipoles with end loading elements forms Jerusalem cross (Figure 1a). The aperture-type Jerusalem cross FSS is practically realized by removing the sections (Figure 1b) corresponding to crossed dipoles and end loading elements on a thick metallic screen (of copper or silver). The transmission response of the grid is mainly controlled by the incident electric field that flow along the edges of vertical inductive sections and across the gaps of horizontal capacitive sections of aperture-type Jerusalem Cross element.

Aperture type Jerusalem Cross FSS array is embedded in the mid-plane of the core of A-sandwich radome panel (Figure 2), for which the skin (Glass epoxy; ε_r =4.0

and $\tan\delta_e$ =0.015) thickness is 0.75 mm. The thickness of the core (Foam; ε_r =1.1 and $\tan\delta_e$ =0.002) optimized for power transmission over the frequency range 8 GHz - 12 GHz is 5.44 mm.

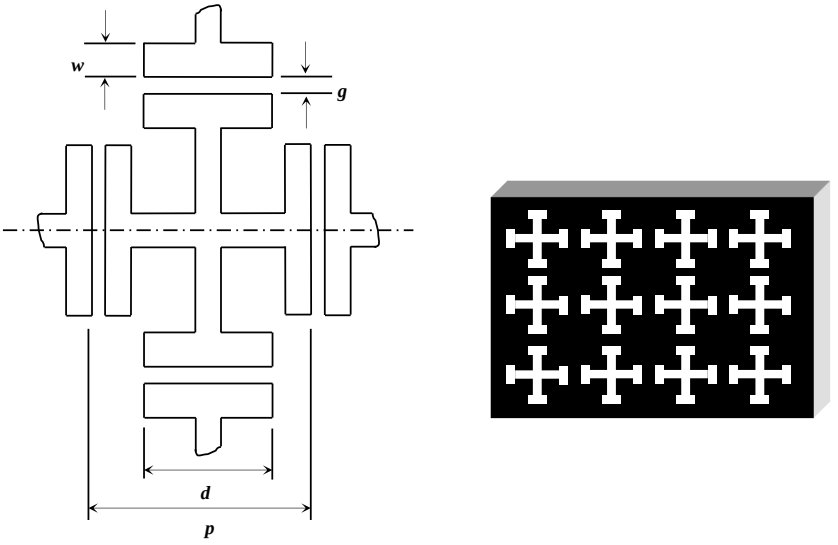

Figure 1: Unit cell of Jerusalem cross FSS and (b) Jerusalem cross FSS (aperture type)

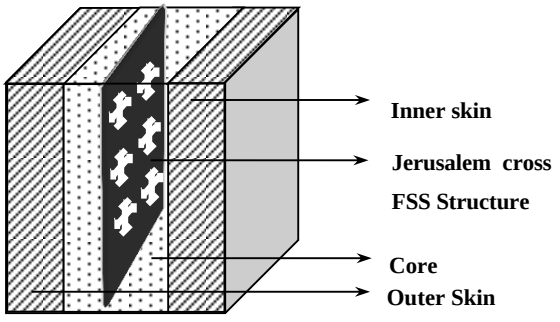

Figure 2: Schematic of A-sandwich radome centrally loaded with aperture-type Jerusalem cross FSS

The inductive susceptance of the Jerusalem cross grid is formulated based on equiv-

alent circuit method and it is incorporated in the modeling of Jerusalem cross FSS embedded A-sandwich wall based on equivalent transmission line method. The design parameters of Jerusalem cross unit cell are: pitch, p; length, d; element width, w; gap width, g; and thickness, t. These design parameters are optimized in such a way that it offers superior EM performance characteristics over the entire X-band, for perpendicular polarization at a given incidence angle (Table 1).

Table 1: Optimized design parameters of Jerusalem cross FSS (Polarization: perpendicular)

Angle of incidence	Width, w (mm)	Length, d (mm)	Gap width, g (mm)	Pitch, p (mm)	Thickness of FSS, t (mm)
0°	0.50	1.1	0.55	2.21	1.35
45°	1.00	4.50	2.40	11.40	1.55
80°	1.80	12.5	1.40	22.60	1.60

The electromagnetic performance parameters power transmission, power reflection and insertion phase delay of the A-sandwich configuration with Jerusalem Cross FSS are computed based on the equivalent transmission line method [Cary (1983)] in conjunction with equivalent circuit model (Anderson (1975); Ohira (2005)]. The entire wall configuration is considered as an equivalent transmission line with different sections corresponding to skin, core and wire grids. The change in the characteristic impedance of the free space and A-sandwich configuration represents a discontinuity in the line, which is a major source of reflection of the wave passing through the structure.

The dielectric layers of A-sandwich wall can be considered as low impedance lines (compared to free space), connected end to end. A matrix consisting of A_i, B_i, C_i, and D_i parameters represents i^{th} dielectric layer. Hence the whole radome wall structure can be represented by a single matrix obtained by the multiplication of matrices corresponding to individual layers.

Let Z_0 be the characteristic impedance of free space. The characteristic impedances of the skin, core and FSS are represented by Z_s, Z_c, and Z_{FSS} respectively. Let Φ be the electrical length corresponding to each layer, which is a function of the complex permittivity (ε^*) of dielectric layer, the angle of incidence (θ) and the thickness of the dielectric layer (d).

The matrix representing each layer of Jerusalem cross FSS embedded A-sandwich

wall are as follows. The outer skin is represented by

$$\begin{bmatrix} A_1 & B_1 \\ C_1 & D_1 \end{bmatrix} = \begin{bmatrix} \cos\Phi_1 & j\frac{z_s}{z_o}\sin\Phi_1 \\ j\frac{z_o}{z_s}\sin\Phi_1 & \cos\Phi_1 \end{bmatrix} \tag{1}$$

In the modified wall configuration, the Jerusalem Cross FSS is located at the mid-plane of the core. Hence the core can be considered to be made up of two identical sections with Jerusalem Cross FSS in between them. Then the first half-section of the core is represented by

$$\begin{bmatrix} A_2 & B_2 \\ C_2 & D_2 \end{bmatrix} = \begin{bmatrix} \cos\Phi_2 & j\frac{z_c}{z_o}\sin\Phi_2 \\ j\frac{z_o}{z_c}\sin\Phi_2 & \cos\Phi_2 \end{bmatrix} \tag{2}$$

Let A_{FSS}, B_{FSS}, C_{FSS} and D_{FSS} be the elements of the matrix representing Jerusalem Cross FSS. Then the Jerusalem Cross FSS is represented by

$$\begin{bmatrix} A_{FSS} & B_{FSS} \\ C_{FSS} & D_{FSS} \end{bmatrix} = \begin{bmatrix} 1 & 0 \\ \frac{1}{jX_r} & 1 \end{bmatrix} \tag{3}$$

Here $X_r$represents the reactance of the Jersualem Cross FSS, which is a function of inductive reactance X and capacitive susceptance B [Anderson (1975)]. Using the equivalent circuit modeling of Jerusalem cross FSS, $X$and B are given by

$$X = \frac{p}{\lambda}\left[\ln\left(\cos ec\left(\frac{\pi w}{2*p}\right)\right)+F\right] \tag{4}$$

$$B = \frac{4d}{\lambda}\left\{\ln\left(\cos ec\left(\frac{\pi g}{2p}\right)\right)+F+\frac{\pi t}{2g}\right\} \tag{5}$$

where F is the correction factor given by,

$$F = \frac{Q\,c^2}{1+Q\,s^2}+\left[\frac{pc}{4\lambda}(1-3s)\right]^2 \tag{6}$$

Here the coefficients Q, c, and s are given by

$$Q = \left[1-\left(\frac{p}{\lambda}\right)^2\right]^{-\frac{1}{2}}-1 \tag{7}$$

where $c = \cos^2\frac{\pi w}{2p}$; and $s = 1-c$.
The second half-section of the core is represented by

$$\begin{bmatrix} A_3 & B_3 \\ C_3 & D_3 \end{bmatrix} = \begin{bmatrix} \cos\Phi_4 & j\frac{z_c}{z_o}\sin\Phi_4 \\ j\frac{z_o}{z_c}\sin\Phi_4 & \cos\Phi_4 \end{bmatrix} \tag{8}$$

The inner skin is represented by

$$\begin{bmatrix} A_4 & B_4 \\ C_4 & D_4 \end{bmatrix} = \begin{bmatrix} \cos\Phi_4 & j\frac{z_c}{z_o}\sin\Phi_4 \\ j\frac{z_o}{z_c}\sin\Phi_4 & \cos\Phi_4 \end{bmatrix} \tag{9}$$

Then the entire radome wall configuration is represented by

$$\begin{bmatrix} A & B \\ C & D \end{bmatrix} = \begin{bmatrix} A_1 & B_1 \\ C_1 & D_1 \end{bmatrix} \begin{bmatrix} A_2 & B_2 \\ C_2 & D_2 \end{bmatrix} \begin{bmatrix} 1 & 0 \\ \frac{1}{jX_r} & 1 \end{bmatrix} \begin{bmatrix} A_3 & B_3 \\ C_3 & D_3 \end{bmatrix} \begin{bmatrix} A_4 & B_4 \\ C_4 & D_4 \end{bmatrix} \tag{10}$$

Using equation (10), the A, B, C and D parameters of the final matrix are computed. The power transmission coefficient is given by

$$\mathbf{P}_{\text{tr}} = \left[\frac{4}{(\text{A}+\text{B}+\text{C}+\text{D})^2}\right] \tag{11}$$

The power reflection coefficient is given by

$$\mathbf{P}_{\text{rf}} = \left[\frac{\text{A}+\text{B}-\text{C}-\text{D}}{\text{A}+\text{B}+\text{C}+\text{D}}\right]^2 \tag{12}$$

The phase distortions are determined by the insertion phase delay (IPD) of the radome wall. For the present radome wall configuration, the inner and outer skin layers, core layers and FSS are cascaded. Hence the insertion phase delay is given by

$$\text{IPD} = -\angle T - \frac{2\pi}{\lambda}\left(2t_s + 2t_c + d_{\text{FSS}}\right)\cos\theta \tag{13}$$

Here $\angle T$ is phase angle associated with the voltage transmission coefficient of the entire radome wall. Here t_s is the thickness of skin layer and t_c is thickness of each section of the core.

3 EM Performance Analysis

The EM performance parameters of the Jerusalem Cross FSS embedded A-sandwich wall are evaluated for perpendicular polarization at normal incidence, 45° and 80°. At normal incidence, power transmission and reflection characteristics of FSS embedded radome are better than that of A-sandwich alone beyond 9.5 GHz (Figures 3 and 4).

The insertion phase delay of Jerusalem cross FSS embedded A-sandwich is much lower than that of A-sandwich wall alone at normal incidence, which is desirable for reducing the phase distortions and boresight error (Figure 5).

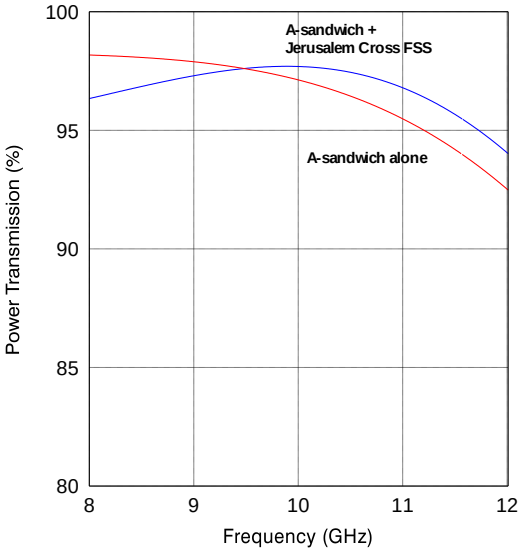

Figure 3: Power transmission efficiency of Jerusalem cross FSS embedded A-sandwich radome and A-sandwich radome alone at normal incidence

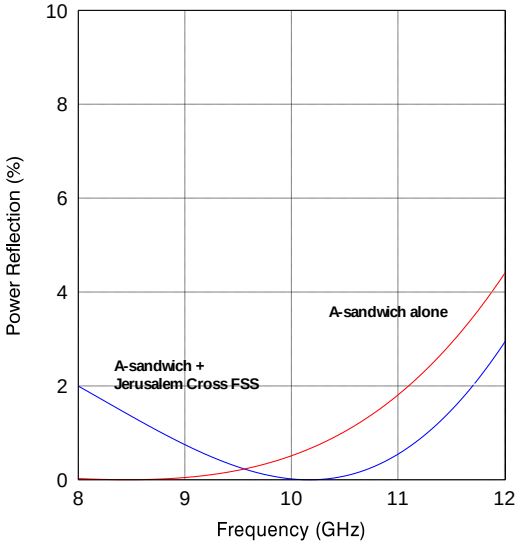

Figure 4: Power reflection characteristics of Jerusalem cross FSS embedded A-sandwich radome and A-sandwich radome alone at normal incidence

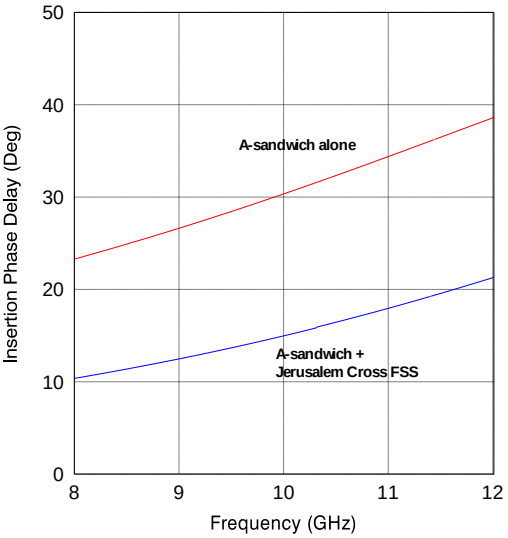

Figure 5: Insertion phase delay characteristics of Jerusalem cross FSS embedded A-sandwich radome and A-sandwich radome alone

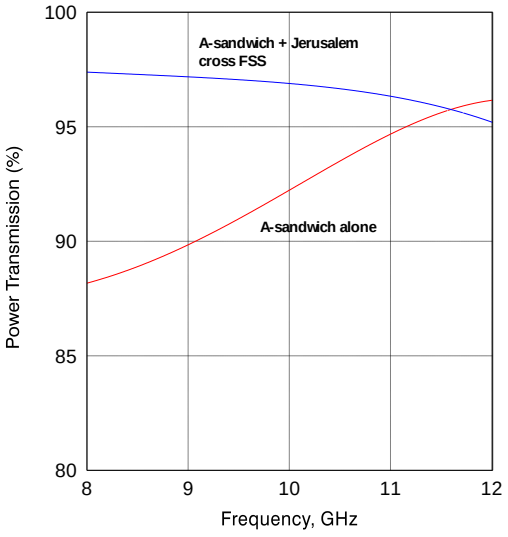

Figure 6: Power transmission efficiency of Jerusalem cross FSS embedded A-sandwich radome and A-sandwich radome alone at 45˚

The EM performance parameters of the new radome wall configuration at 45˚ are shown in Figs. 6-8. The power transmission efficiency of the Jerusalem Cross FSS embedded A-sandwich radome wall is well above 95% and it is much better than that of A-sandwich alone (Figure 6). The power reflection of the FSS embedded structure is well below 5% and it is much lower than that of A-sandwich alone (Figure 7). Similarly the insertion phase delay of the FSS embedded radome wall is lower than that of A-sandwich alone (Figure 8). It is noted that the EM performance parameters of FSS embedded radome wall at 45˚ is much better than that at normal incidence case.

Figures 9-11 show the EM performance parameters of the Jerusalem cross FSS embedded A-sandwich radome panel and A-sandwich radome alone at the high incidence angle 80˚. The power transmission efficiency of Jerusalem cross FSS embedded A-sandwich is much higher than that of A-sandwich radome alone. The power reflection and insertion phase delay of Jerusalem cross FSS embedded A-sandwich radome panel are much lower than that of A-sandwich radome alone. The EM analysis shows that the EM performance of Jerusalem cross FSS embedded panel is far superior to that of A-sandwich alone at normal incidence, intermediate incidence angle 45˚ and high incidence angle 80˚.

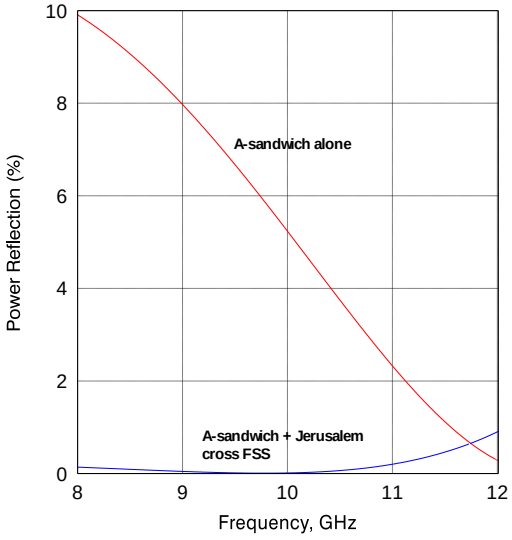

Figure 7: Power reflection characteristics of Jerusalem cross FSS embedded A-sandwich radome and A-sandwich radome alone at 45˚

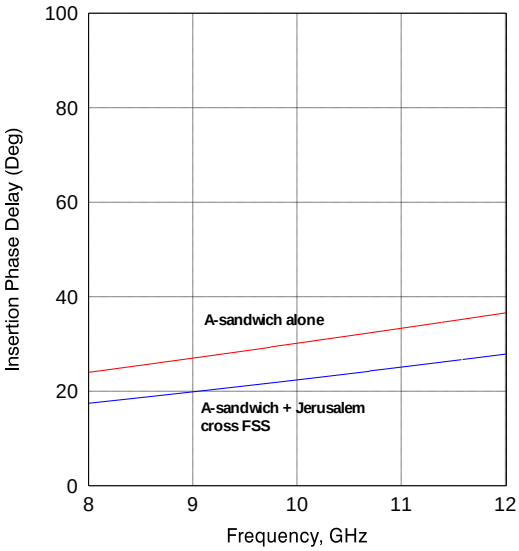

Figure 8: Insertion phase delay characteristics of Jerusalem cross FSS embedded A-sandwich radome and A-sandwich radome alone at 45°

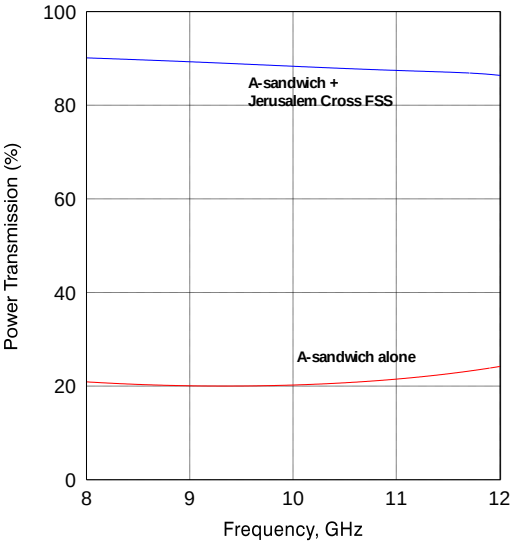

Figure 9: Power transmission characteristics of Jerusalem cross FSS embedded A-sandwich radome and A-sandwich radome alone at 80°

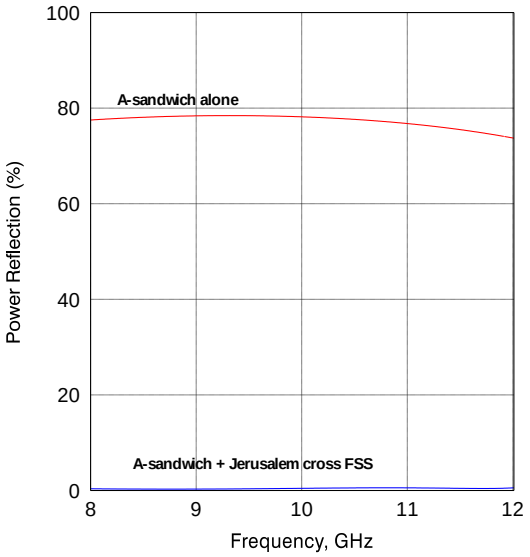

Figure 10: Power reflection characteristics of Jerusalem cross FSS embedded A-sandwich radome and A-sandwich radome alone at 80˚

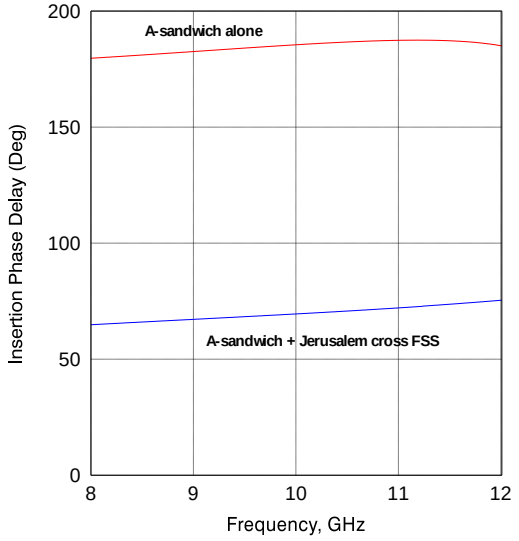

Figure 11: nsertion phase delay characteristics of Jerusalem cross FSS embedded A-sandwich radome and A-sandwich radome alone at 80˚

4 Conclusions

Enhancement of EM performance parameters of A-sandwich radome over X-band using aperture-type Jerusalem cross FSS is presented. EM performance analysis indicates that Jerusalem cross FSS embedded A-sandwich radome has superior EM performance characteristics at normal incidence, 45˚ and 80˚ over the entire X-band. Further this novel structure has overcome the major limitation of conventional A-sandwich radome, that is poor EM performance at high incidence angles. Considering the excellent EM performance characteristics over a wide range of incidence angles for a given frequency band, it can be used in the design of normal incidence (hemispherical/ cylindrical radomes), near–normal incidence radomes (paraboloidal radomes), and highly streamlined airborne nosecone radomes. Further, the presence of thick metallic FSS in the radome wall offers more structural rigidity beneficial for aerospace applications.

References

Anderson, I. (1975): On the theory of self-resonant grids. *The Bell System Technical Journal*, vol. 54, pp. 1725-1731.

Basiry, R.; Abiri, H.; Yahaghi, A. (2011): Electromagnetic performance analysis of omega type metamaterial radome. *International Journal of RF and Microwave Computer-Aided Engineering,* vol. 21, no. 6, pp. 665-673.

Cary, R. H. J. (1983): *Radomes, The Handbook of Antenna Design.* Peter Peregrinus, London, ISBN 0-906048-87-7, p. 930.

Choudhury, B.; Bisoyi, S.; Jha, R.M. (2012): Emerging trends in soft computing for metamaterial design and optimization. *Computers, Materials & Continua,* vol. 31, no. 3, pp. 201-228.

Cory, S.; Lee, Y. J.; Hao, Y.; Parini, C. G. (2007): Use of conjugate dielectric and metamaterial slabs as radomes. *IET Microwaves, Antennas, and Propagation,* vol. 1, no. 1, pp. 137-143.

Costa, F.; Monorchio, A. (2012): A frequency selective radome with wideband absorbing properties. *IEEE Transactions on Antennas and Propagation*, vol. 60, no. 6, pp. 2740-2747.

Frenkel, A. (2001): Thick metal dielectric radome. *Electronics Letters,* vol. 38, no. 23, pp. 1374-1375.

Kozakoff, D. J. (2010): *Analysis of radome enclosed antennas* , Artech House, Norwood, USA, ISBN 13: 978-1-59693-441-2, p. 318.

Latrach, M.; Rmili, H.; Sabatier, C.; Seguenot, E; Toutain, S. (2010): Design of a new type of metamaterial radome low frequencies. *Microwave and Optical*

Technology Letters, vol. 52, no. 5, pp. 1119-1123.

Lin, B.-Q.; Li, F.; Zheng, Q.-R.; Zen, Y.-S. (2009): Design and simulation of a miniature thick-screen frequency selective surface radome. *Progress in Electromagnetics Research*, vol. 138, pp. 537-553.

Munk, B. A. (2005): *Frequency Selective Surfaces: Theory and Design.* Wiley, New York, USA, ISBN 0471723762, p. 440.

Nair, R. U.; Jha, R. M. (2009): A novel Jerusalem cross FSS embedded A-sandwich radome for aerospace applications. *IEEE Applied Electromagnetics Conference AEMC 2009*, Paper No.: CEM-8-2621, 4p.

Narayan, S.; Shamala, J. B.; Nair, R. U.; Jha, R. M. (2012): Electromagnetic performance analysis of novel multiband metamaterial FSS for millimeter wave radome applications. *Computers, Materials & Continua,* vol. 31, no. 1, pp. 1-16.

Ohira, M.; Deguchi, H.; Tsuji, M.; Shigesawa, H. (2005): Analysis of frequency selective surface with arbitrary shaped element by equivalent circuit model. *Electronics and Communications in Japan*, part 2, vol. 88, pp. 9-17.

Wu, T. K. (1995): *Frequency Selective Surface and Grid Array.* Wiley, New York, ISBN 0471311898, p. 331.